Available online at www.sciencedirect.com
SCIENCE DIRECT
International Journal of Heat and Fluid Flow 26 (2005) 883–893
International Journal of HEAT AND FLUID FLOW
www.elsevier.com/locate/ijhff

Turbulence modification in vertical upward annular flow passing through a throat section

Kenji Yoshida *, Tadayoshi Matsumoto, Isao Kataoka

Graduate School of Engineering, Mechanical Engineering, Osaka University, 2-1 Yamada-Oka, Suita, Osaka 565-0871, Japan

Available online 8 November 2005

Abstract

Experimental studies on the turbulence modification in annular two-phase flow passing through a throat section were carried out. The turbulence modification in multi-phase flow due to the interactions between two-phases is one of the most interesting scientific issues and has attracted research attention. In this study, the gas-phase turbulence modification in annular flow due to the gas–liquid phase interaction is experimentally investigated. The annular flow passing through a throat section is under the transient state due to the changing cross sectional area of the channel and resultantly the superficial velocities of both phases are changed compared with a fully developed flow in a straight pipe. The measurements for the gas-phase turbulence were precisely performed by using a constant temperature hot-wire anemometer, and made clear the turbulence structure such as velocity profiles, fluctuation velocity profiles. The behavior of the interfacial waves in the liquid film flow such as the ripple or disturbance waves was also observed. The measurements for the liquid film thickness by the electrode needle method were also performed to measure the base film thickness, mean film thickness, maximum film thickness and wave height of the ripple or the disturbance waves.

Keywords: Turbulent modification; Annular flow; Wavy interface; Throat section turbulence structure

1. Introduction

Gas and liquid phase in two-phase annular flow is supposed to be affected each other by another phase compared with single-phase flow. The dynamic interaction between gas and liquid phase through the interfacial waves in annular two-phase flow has attracted research attention, because the investigation for the thermo-hydrodynamic structure and the characteristics of the gas-core flow and the liquid film flow with wavy interface is very important concerned with the special phenomena such as the turbulent modifications of gas-core flow, resultant entrainment or deposition of droplets or formation of the disturbance wave on the liquid film flow.

Many studies on turbulence modification in multiphase flow caused by a second phase are investigated, the majority of these studies report on gas–solid, liquid–solid, or bubbly liquid–gas two-phase flow system. Gore and Crowe (1989) pointed out that from the data where the dispersed phase was solids, two types of behavior occurs, enhancement or suppression of turbulence, depending on the ratio of particle size to turbulent length scale. Hestroni (1989) studied the interaction between solid particles and the turbulence of the carrier fluid. Kajishima et al. (1999) investigated the numerical analysis of turbulence eddies caused by solid particles using DNS method.

Some published literatures reported on the turbulence modifications of the gas-core in annular flow. Azzopardi and Teixeira (1994a) measured two simultaneous components of gas-core velocity in annular flow. They measure the velocity of 1 mm polystyrene tracer particles injected into the gas flow by using a LDV system, and also measured the sizes and velocity of droplets using the PDA system (Azzopardi and Teixeira, 1994b). Fore and Dukler (1995) measured the droplets size and velocity distribution in gas–liquid annular up flow using PDA system. Turbulence intensity for annular gas–liquid flow were examined

* Corresponding author. Tel./fax: +81 6879 7259.
E-mail address: yoshida@mech.eng.osaka-u.ac.jp (K. Yoshida).

0142-727X/$ - see front matter © 2005 Elsevier Inc. All rights reserved.
doi:10.1016/j.ijheatfluidflow.2005.10.008

and contrasted with values from gas–solids flow by Azzopardi (1999). He suggested that the rough wavy interface of the liquid film and droplets, which are slow moving just after their creation from the liquid film, should be the contributions of turbulence augmentation in annular flow.

In this paper, experimental studies were made to investigate the dynamic interaction between gas core flow and liquid film flow with wavy interface such as ripple or disturbance wave in air/water annular flow in a vertically arranged round tube. Typical two types of flow channel were used as the test channel. The first one is the straight pipe, whose cross sectional area is the constant. The second one is a circular pipe with a throat section. The cross sectional area of this channel is gradually reducing (nozzle part), constant (throat part) and expanding (diffuser part), where the superficial velocity for gas and liquid phases change along with the flow direction. Air and water were used as the working fluids of gas and liquid phases, respectively. The experiments for annular flow in a straight pipe were firstly carried out and accumulate the fundamental reference data for annular flow to understand the characteristic phenomena such as the turbulence modification due to the interfacial interaction of gas and liquid phases and the dynamic behavior of the interfacial waves. The transient behavior of the interfacial waves on liquid film such as disturbance waves and ripple waves were observed by using a digital camera and a high-speed video camera system. The time-series of axial velocity component for gas-core flow were precisely measured by using a constant temperature hot-wire anemometer. The measurement for the liquid film thickness by using a point-electrode resistivity probe was also carried out. Secondary, the experiments for the annular flow passing through a throat section were carried out to investigate the transient behavior of the gas-core flow and the liquid film flow. The velocity measurements for the gas-core flow and the measurements for the liquid film thickness at the nozzle, throat and diffuser part were carried out. The direct observations for the interfacial wave structure passing through the throat section were also carried out by using a high-performance digital camera.

2. Experimental apparatus

2.1. Flow loop

The schematic drawing of the experimental flow loop is shown in Fig. 1. The flow channel was a vertical arranged clear acrylic circular pipe of 20.03 mm inner diameter, and about 7.6 m lengths. The flow direction was upward. The symbols in Fig. 1, "T", "DP", "P" and "F" indicate the thermocouples, differential pressure gauge, pressure gauge and flow meter, respectively. The test channel (measurement station), which is represented as "4" in this figure, was attached at about 4.8 m height from the bottom of the channel. In this study, two types of the test channel were used. The first one is the straight pipe of inner diameter is 20.03 mm, has a constant inner diameter. This is the

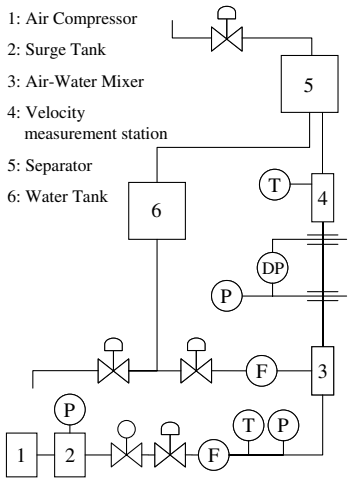

Fig. 1. Schematic drawing of the experimental flow loop.

fundamental test channel to measure the equilibrium state of annular flow. The second one is the round tube with a throat section, where the cross sectional area of the pipe gradually reduce (nozzle part, $\phi = 20.03\ \text{mm} \rightarrow \phi = 10.0\ \text{mm}$, $L = 100\ \text{mm}$), constant (throat part, $\phi = 10.0\ \text{mm}$, $L = 20\ \text{mm}$) and expand (diffuser part, $\phi = 10.0\ \text{mm} \rightarrow \phi = 20.03\ \text{mm}$, $L = 100\ \text{mm}$) along the flow direction. This channel has relatively rapid change of cross sectional area, so, the acceleration and the deceleration of fluids should be occurred in these parts. The transient behavior of gas-core turbulence and liquid film flow would be observed around the throat section. Dried air and filtered water under the normal temperature and the atmospheric pressure were used as the working fluids. The air/water mixer, which is represented as "3" in Fig. 1, is attached at the bottom part of the channel. Dried air supplied from the scroll compressor, which is represented as "1", is once stored in the pressure tank ("2") to keep from the flow rate surging, and introduced to the air/water mixer. The water from the head tank represented as "6" is introduced to the air/water mixer, and injected through the eight pin-holes of 2.0 mm I.D. pricked on the pipe wall of the mixer. Before mixing the air and water, the flow rate of air and water were regulated and measured separately by the variable-area flow meter and the ultrasonic flow meter, respectively. The measurement station for the gas-phase velocity or liquid film thickness was attached at about 4.8 m height from the bottom. It was about 240 diameters height from the bottom of the channel. For the range of the applied flow rates, the height was sufficient to reasonably reach to the equilibrium state at the inlet of the test channel.

2.2. Velocity measurements

The gas-phase velocity measurement was made by using a constant temperature hot-wire anemometer (CTA). The velocity measurement by using a hot-wire anemometer

has some advantages in the point of direct measuring for the gas-phase velocity field, without using the tracer particles. And the turbulence energy spectrum analysis is easily possible because of the time-series of the velocity data can be acquired continuously. The U-type hot-wire probe (KANOMAX 0248-T5, $\phi = 5$ μm, $l = 1.0$ mm) of tungsten wire is inserted into the test sectional pipe. The over heating ratio was set to be 1.5. The CTA system (KANOMAX CTA System 7000) consists of the CTA unit, the linearizer unit, and the temperature compensation unit. The linearizer unit makes directly the CTA voltage signal to be the proportional to the real velocity. The temperature compensation unit allows the gentle temperature decreasing due to the slight vaporization of liquid phase. The hot-wire probe was set up to be able to traverse on the radial direction precisely by using a micrometer in a micron meter precision and can be fixed at any radial position. In the case of pipe flow like this study, U-type probe can measure the instantaneous axial velocity component by setting the hotwire perpendicular direction against the main stream direction. The uncertainty of this CTA system used in this study is 0.07% at 10 m/s wind velocity or less.

From the acquired time-series of the axial velocity information, we can calculate the turbulent structural parameter such as the time-averaged axial velocity profile, the fluctuation velocity profile, the energy spectrum, and the auto-correlation coefficient of the fluctuation velocity component. The velocity signals from the CTA system were acquired by a A-D converter (National Instruments, PCI-MIO-16E-1). The sampling frequency of data acquisition was set to be 100 kHz, which is adequate to capture the turbulence fluctuation (Raynolds, 1974). Data analysis was performed by using a data analysis software (National Instruments LabVIEW6i). The sampling period was set to about 40 s for each case.

2.3. Measurements for liquid film

To make clear the interaction of the wavy interface moving on the liquid film flow and the gas-phase turbulence, the liquid film thickness was also measured by using the point electrode needle method, which is based on the method developed by Serizawa et al. (1992).

The measuring setup is nearly the same, which is for the measurement of gas-phase velocity profile. For the film thickness measurements, the hot-wire probe was replaced to the point resistivity probe. On the opposite side on the inner surface of the test channel, the cathode electrode, which is grounded, was buried in the pipe wall. The surface of the cathode electrode is polished to make the electrode and pipe wall smooth and not to make the difference in height level each other. A point-electrode probe is made of stainless steel wire with a diameter of 0.2 mm. The stainless wire was inserted into Teflon-insulated tube of 0.36 mm diameter. The wire was coated with insulating enamel except for its tip, and it was dried up to ensure a well insulation at 200° centigrade. This wire was inserted into sheath stainless steel tube. The electrode probe was mounted on a traverse system with a micrometer and can be fixed at any radial position from the inner surface of the pipe wall in micron-meter precision. The tip of the probe, which is the anode electrode, is can be moved into the liquid film flows. As the tip of the probe was moved, the time fraction contacting with the liquid takes place is detected, and is the probability that the film thickness is greater than the distance between the tip of wire and pipe wall. This measurement can provide the information of the minimum, maximum, time-averaged mean thickness and interfacial wave height of liquid film with reasonable reliability. The uncertainty of the measurement of the film thickness is 1 micron meter. The series of the electric signal from the electrode probe was acquired by using a A-D converter. The sampling frequency of the data acquisition was set to be 10 kHz. The data sampling period was set to 60 s for each case.

The direct observations for the liquid film behavior by using a high speed-video camera (Photoron, FastCAM-Net) was also carried out to make visually clear the dynamic behavior of the interfacial waves. The dynamic behavior and the structure of the ripple or the disturbance wave on gas–liquid interface were visually made clear by backlight image technique. The shutter speed and the flame rate of the high-speed video camera were set to 1/5000 s and 1000 fps, respectively, which were quick enough to capture the moving interfacial waves.

3. Experimental condition

In this study, two types of the test section were used. The first one is a straight pipe of 20.03 mm inner diameter. We call this "20 mm pipe." The second one is a pipe with a throat section. The experiments were carried out for the cases changing the superficial velocities of gas and liquid phases, j_G and j_L, respectively. In this study, the superficial velocity, which is defined of 20 mm pipe, of gas-phase was changed approximately from $j_{G/20} = 15.5$ m/s to 26.5 m/s. The superficial velocity of liquid-phase was changed from $j_{L/20} = 0.75$ cm/s to 1.25 cm/s, which is also defined of 20 mm pipe.

The experimental conditions of this study were restricted to "the regime of annular flow without entrainment," which was the ripple region or the disturbance wave region without entrainments from the liquid film, because of making clear the effect of wavy interface moving on the liquid film on the turbulence modification in the gas-phase flow. The flow regime boundaries indicating the with or without entrainments from the liquid film are represented by Kutateladze (1972), Steen and Wallis (1964) and Ishii and Grolmes (1975). The experimental conditions carried out in this study were restricted in the regime where there are no entrainments from the liquid film.

Fig. 2 shows the schematic drawing of the test channel with a throat section. This test section consists of three parts of the nozzle, throat and diffuser part. The cross

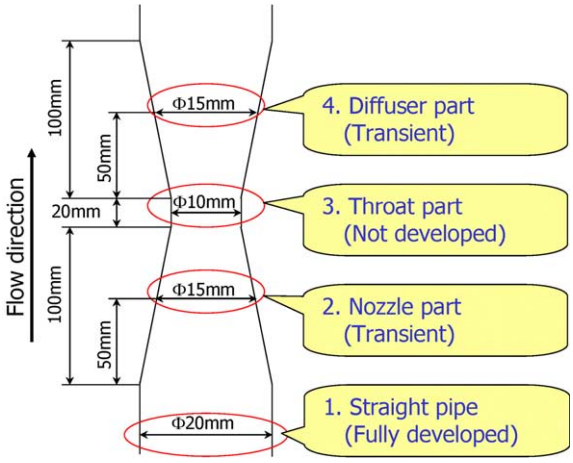

Fig. 2. Schematic drawing of the test channel with a throat section.

sectional area of the channel is gradually reduced in nozzle part, constant at throat part, and gradually increased in diffuser part along the flow direction. The length of each part is 100 mm, 20 mm and 100 mm, respectively. Its inner diameter changes from 20 mm to 10 mm in nozzle part, and 10 mm to 20 mm in diffuser part, respectively. The diameter of the throat part is 10 mm. In these parts, the cross sectional area has relatively rapid change, resultantly, the superficial velocity is accelerated or decelerated rapidly in nozzle and diffuser part. So, the annular flow is in transient state, not in developed state in this test channel.

4. Results and discussion

4.1. Results for fully developed flow in straight pipe

4.1.1. Time-averaged and fluctuation velocity profiles

Fig. 3(a) shows the measured time-averaged gas-phase velocity profiles in annular flow flowing in a straight pipe. The flow is fully developed. The horizontal axis represents the non-dimensional radial position, and the vertical axis means the time-averaged axial velocity, which was non-dimensionalized by the superficial gas velocity. The vertical axis of $r/R = 0$ indicates the central axis of the pipe. The result for the case of the single-phase flow ($j_L = 0.0$ cm/s) was also measured and plotted in solid-circled line. In the case for the single-phase flow, the measured velocity profiles have a agreement with Laufer's data (1954), which is the well known accurate data for the single-phase turbulence flow in a circular tube. The error between the measured data and Laufer's data is at the worst 2.6% or less. This can make a confirmation that the velocity measurements in the present experiments were precisely performed and has a reasonable accuracy. In the case for the annular flow, the velocity profiles are modified to sharpened shape. The velocity near the central axis increases and the velocity near the pipe wall decreases. This modification becomes significant as the flow rate of the liquid film becomes larger.

Fig. 3(b) shows the measured fluctuation velocity profiles of gas-phase in fully developed annular flow, which

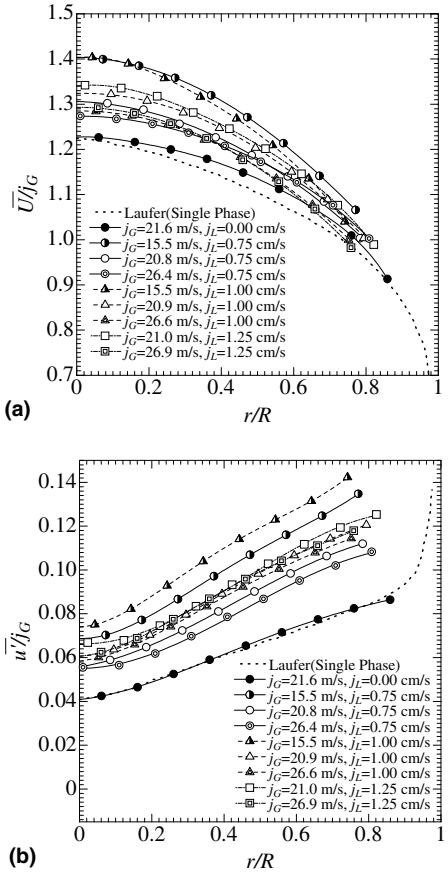

Fig. 3. Time-averaged and fluctuation velocity profiles of gas-core in fully developed annular flow flowing in straight a pipe of $\phi = 20$ mm. (a) Time averaged gas-phase velocity profiles in the fully developed annular flow. (b) Fluctuation velocity profiles in the fully developed annular flow.

is non-dimensionalized by divided by the superficial gas-phase velocity. The experimental data for the single-phase flow and the annular flow are plotted in Fig. 3(b). The published data for single-phase flow measured by Laufer (1954) is also drawn. In the case for single-phase flow, the experimental data has a good agreement with Laufer's data. In the case for the annular flow, the fluctuation velocity becomes larger than that of the single-phase flow through the all-radial position. This enhancement of gas-phase turbulence fluctuation becomes significant as the flow rate of liquid film becomes larger. This additional turbulence fluctuation is due to the wavy interface on liquid film flow.

4.1.2. Energy spectrum and auto-correlation for fluctuation velocity component

Fig. 4(a) shows the one-dimensional energy-spectrum density function for the axial fluctuation velocity component on the central axis for the single-phase flow and the annular flow. The horizontal axis indicates the frequency of turbulence fluctuation, and the vertical axis means the one-dimensional energy spectrum density function for the fluctuation component. The FFT algorism was used to

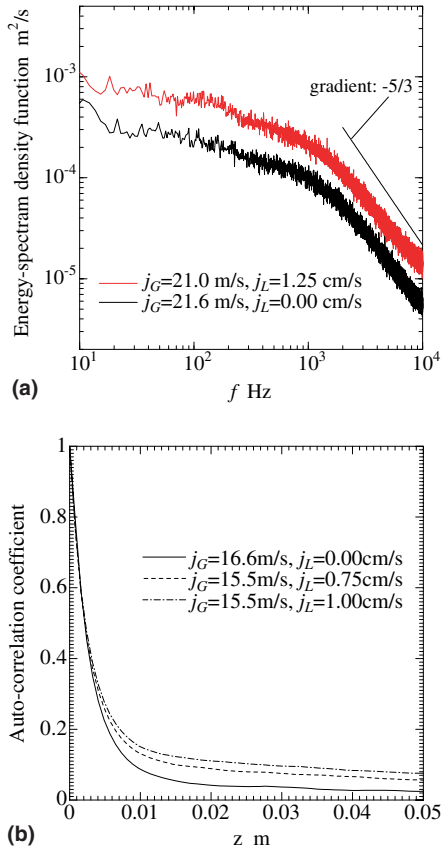

Fig. 4. Energy spectrum and auto-correlation for the fluctuation velocity component in the fully developed annular flow flowing in a straight pipe of $\phi = 20$ mm. (a) One-dimensional energy spectrum density function. (b) Auto-correlation coefficient of fluctuation velocity.

evaluate the energy-spectrum density function from the original fluctuation velocity data, which was acquired on the central axis of the pipe. The typical two cases for annular flow ($j_G = 21.0$ m/s, $j_L = 1.25$ cm/s) and single-phase flow ($j_G = 21.6$ m/s, $j_L = 0.00$ cm/s) were plotted. For each case, superficial velocity of gas-phase was set to nearly the same condition. The solid line in the figure indicates the inertial sub-range spectrum, which is introduced from Kolmogorov's theory. The gradient of this line is $-5/3$ power.

From Fig. 4(a), the energy spectrum in annular flow becomes larger in whole range compared with the single-phase flow. This corresponds to the increased fluctuation velocity in annular flow as shown before in Fig. 3(b). Especially, increased energy-spectrum is relatively significant in the frequency range of 10^1–10^3 Hz, which is relatively low frequency regime. This indicates that the low frequency vortex, which has relatively large size, is preferentially enhanced in gas-core turbulence in annular flow due to the wavy interface moving on the liquid film flow. On the other hand, for both cases of single-phase flow and annular flow, the energy-spectrum gradient in the inertial sub-range, which is high-frequency region of $f > 10^3$ Hz, fit well $-5/3$ power, which has good agreements with Kolmogorov's theory. This means the energy equilibrium relations or energy dissipation mechanism in the inertial sub-range in annular flow is the same with the single-phase flow.

Fig. 4(b) shows the auto-correlation coefficients for the fluctuation velocity component on the central axis for the single-phase flow and the annular flow. The FFT and IFFT algorism were used to evaluate the auto-correlation coefficient from the acquired original fluctuation velocity data. The horizontal axis means the distance from the reference point, which was calculated by multiplying the time-averaged main-stream velocity and the time difference of data acquisition. This is based on the assumption of the ergodic data series. The vertical axis indicates the auto-correlation coefficient for the fluctuation velocity component, which was non-dimesionalized auto correlation function by mean square of the fluctuation velocity. Three typical cases for single-phase flow $j_G = 16.6$ m/s, $j_L = 0.00$ cm/s) and annular flows ($j_G = 15.5$ m/s, $j_L = 0.75$ cm/s; and $j_G = 15.5$ m/s, $j_L = 1.00$ cm/s) are plotted. For each case, the superficial velocity of gas-phase was set to be nearly the same conditions.

From Fig. 4(b), it is noted that the auto-correlation coefficient for annular flow becomes larger compared with single-phase flow in the range of $z > 0.005$ m. As the superficial velocity of liquid-phase increased, this tendency becomes significant. This indicates that the integral scale (macro scale) of turbulence vortex becomes larger in the annular flow compared with the single-phase flow. It is also noted that the gas-phase turbulence in annular flow is modified and has a coherency in the range of $z > 0.005$ m. This should be affected by gas–liquid wavy interface that is periodically moving on the liquid film flow.

The ripple is thought to be the main factor concerning this turbulence excitation. The spatial size of the ripple is about 0.005 m, which is clear from the photos in Fig. 5(a), (c) and (e). This spatial size corresponds to the frequency range of ~1000 Hz, which is calculated from the superficial gas velocity. This has reasonable agreement with the auto-correlation coefficient shown in Fig. 4(b). Of course, the disturbance waves itself might be strongly effective on the turbulence modification of gas-core, but its appearance is too rare in the present experimental condition. So, the statistical analysis performed in this study, the effect of disturbance wave tends to be submerged.

4.1.3. Direct observation for gas–liquid wavy interface

Fig. 5 shows the direct photograph of the dynamic behavior of the wavy interface on the liquid film flow. The photos of (a)–(f) represent the photos for the cases changing the superficial velocities of the liquid-phase and gas-phase. The shutter speed of the high-speed video camera was set to 1/5000 s, which was short enough to capture clearly the motion and shapes of the ripple or the disturbance wave propagation on the liquid film interface. In these figures, (a) and (b) show the cases with keeping the superficial gas velocity j_G on 15.5 m/s, but changing the superficial liquid velocity j_L on 0.75 or 1.00 cm/s, respectively. (c) and (d) show the cases of keeping j_G about

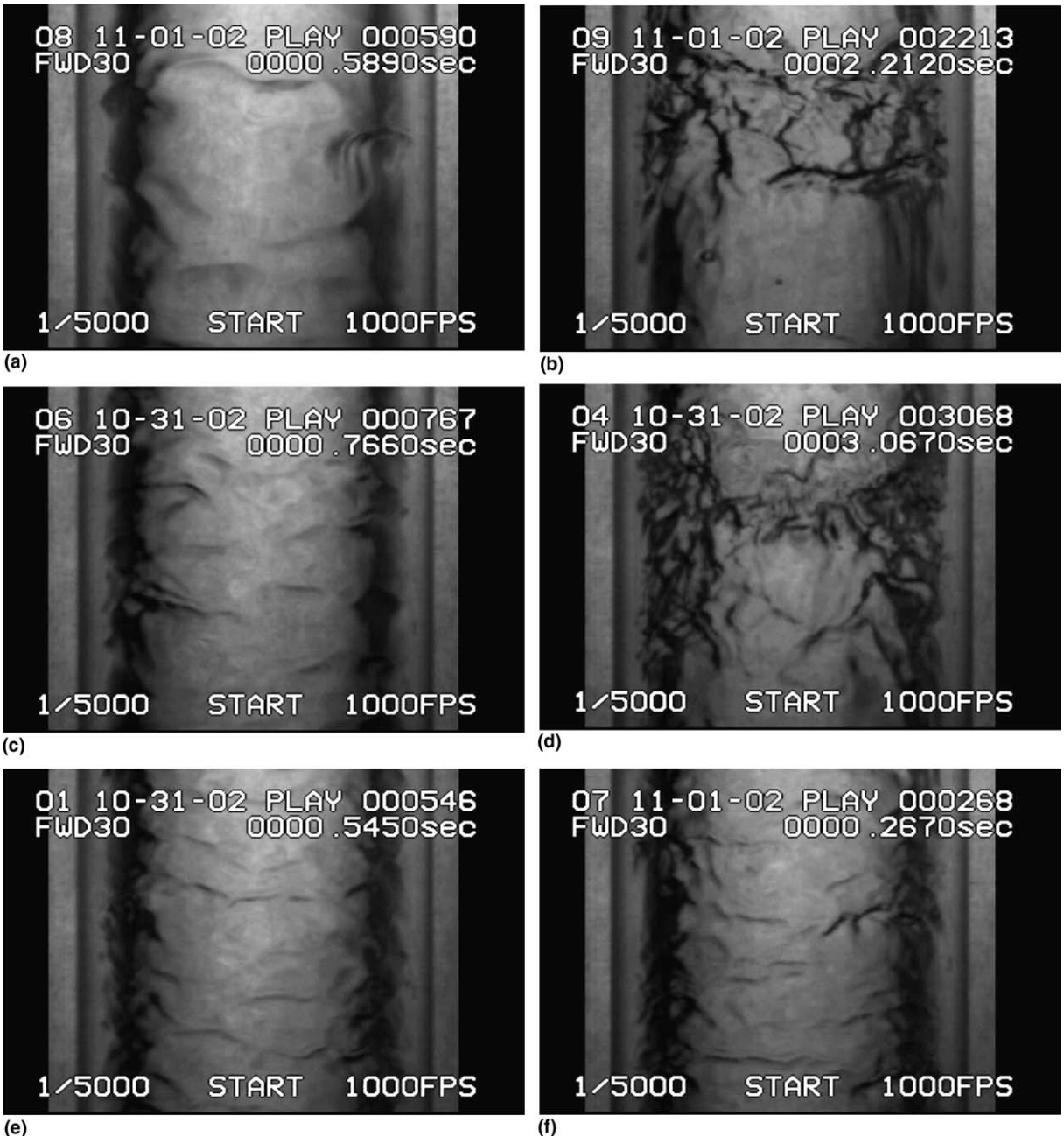

Fig. 5. Direct photographs of wavy interface on liquid film flow. (a) $j_G = 15.5$ m/s, $j_L = 0.75$ cm/s. (b) $j_G = 15.5$ m/s, $j_L = 1.00$ cm/s. (c) $j_G = 20.8$ m/s, $j_L = 0.75$ cm/s. (d) $j_G = 21.0$ m/s, $j_L = 1.25$ cm/s. (e) $j_G = 26.4$ m/s, $j_L = 0.75$ cm/s. (f) $j_G = 26.9$ m/s, $j_L = 1.25$ cm/s.

20.8 m/s, and (e) and (f) represent the cases of j_G equal about 26.4 m/s, but changing the j_L on 0.75 or 1.25 cm/s, respectively.

As shown in Fig. 5(b) and (d), it is noted that the disturbance wave, which has very complicated wrinkle structure and large propagating velocity, were observed at rare intervals on the liquid film flow. The disturbance waves occur periodically like the pulses in the frequency of about 0.3–2 Hz in these cases. From the image processing method, it was noted that the propagating velocity of the ripple is increases as the flow rate of gas and liquid increases. The interfacial velocity of the ripple is ranged from 0.338 to 0.415 m/s in the case of the superficial gas velocity j_G is 15.5 m/s, 0.416–0.516 m/s in the case of j_G is 20.8 m/s, and 0.517–0.712 m/s in the case of j_G is 26.4 m/s, respectively. This was about 1.1–2.1 times of the mean velocity of the liquid film. From the Fig. 5, the spatial size of the ripple wave is around 0.005 m, so, the corresponding wave frequency is 70–150 Hz, which is calculated from the wave propagating velocity. The propagation velocities of the disturbance waves reach up to 3–10 times of that of the ripple waves. The disturbance wave appears in the condition of relatively high superficial liquid velocity and low superficial gas velocity. In the case of (f), disturbance waves rarely

occur, even though the superficial liquid velocity is the same with cases of (b) and (d). In the cases of (c) and (e), in which the superficial liquid velocity is lower, only ripple wave was observed on liquid film flow. It is also noted from figs of (a), (c) and (e), the ripple waves become minute structure as the superficial gas velocities becomes larger.

4.1.4. Measurements for liquid film thickness

Fig. 6 show the experimental results for the measurements of the liquid film thickness. The horizontal axis means the distance between the tip of the point-electrode resistivity probe and the pipe wall. The vertical axis means the measured time-averaged void fraction, which indicates the fraction of the time period when the probe tip contacts with the gas-phase takes place. The mean film thickness was determined as the distance from the pipe wall that the time-averaged void fraction is 50%. The base film thickness was determined as the distance that the void fraction just rises up from zero. The maximum thickness of the liquid film, which might be the maximum height of disturbance waves or ripple waves, was determined as the distance from the wall that the void fraction reaches up to 99.8%.

From Fig. 6, it is noted that the mean film thickness decreases as the flow rate of gas-phase increases. It is also noted that the mean thickness of the liquid film mainly depends on the gas flow rate, but does not depend on the liquid flow rate; the mean thickness has nearly the same value when the gas flow rates were the same conditions. On the other hand, minimum or maximum thickness of liquid film changes as the liquid flow rate changes. As the liquid flow rate increases, the gradient of curves drawn in Fig. 6 indicating the void fraction tends to decrease. Especially, this tendency becomes significant in the region where the void fraction is near 100%. This means the maximum thickness of the liquid film increases radically. This tendency corresponds to the appearance of the disturbance wave on the liquid film flow. The disturbance wave height might be 10–50 times of mean thickness of liquid film. Meanwhile, the thickness of base film or mean thickness does not change so much even though the disturbance wave appears.

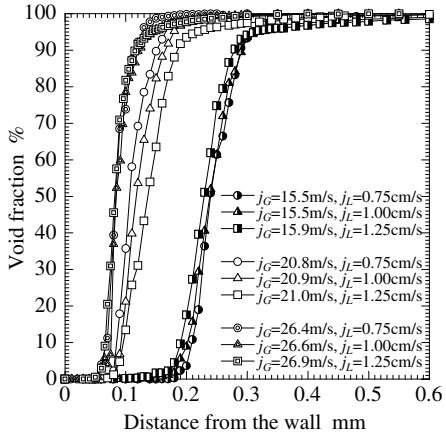

Fig. 6. Liquid film thickness in the fully developed annular flow in the straight pipe of $\phi = 20.03$ mm I.D.

4.2. Results for transient annular flow passing through the throat section

4.2.1. Direct observation for gas–liquid wavy interface

To make clear visually the transient behavior of the gas–liquid interface passing through the nozzle, throat and diffuser part, the direct observations using a high performance digital camera (Nikon D1) were firstly carried out. For the observation, the test channel was made of transparent acrylic block. To keep from image distortion due to the light reflection, the test channel (nozzle, throat and diffusion part) was hollowed out an acrylic rectangular solid. Typical cases of the captured back-light images taken by digital camera are shown in Fig. 7. The shutter speed was set to 1/16,000 s, which was enough short to capture clearly the interfacial waves moving on the liquid film with high velocity.

Fig. 7 shows the typical photos for cases of the superficial velocity of gas-phase, which was defined in 20 mm diameter pipe ($j_{G|20}$), were set to nearly 16.5 m/s. (a)–(d) in each figures indicate the cases for the superficial velocity of liquid phase, which was defined in 20.03 mm diameter

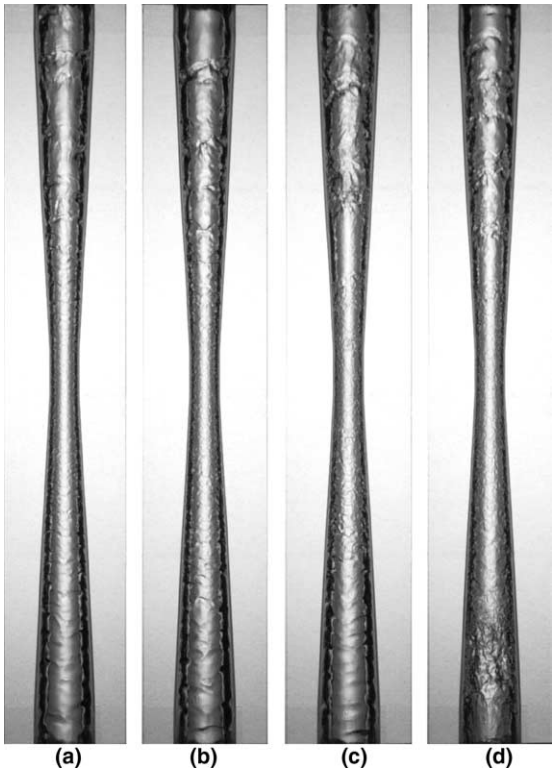

Fig. 7. Captured photos of gas–liquid interface passing through the throat section. (a) $j_{G|20} = 16.2$ m/s, $j_{L|20} = 0.75$ cm/s, (b) $j_{G|20} = 16.5$ m/s, $j_{L|20} = 1.00$ cm/s, (c) $j_{G|20} = 16.5$ m/s, $j_{L|20} = 1.25$ cm/s and (d) $j_{G|20} = 17.1$ m/s, $j_{L|20} = 5.00$ cm/s.

pipe ($j_{L|20}$), were changed to 0.75 cm/s, 1.00 cm/s, 1.25 cm/s and 5.00 cm/s, respectively.

The cross sectional area in the throat part is consequently about 1/4 of the straight pipe. The flow rate of gas-phase and liquid-phase were set to be nearly the same of the experiments for straight pipe. So, the appearance of the disturbance waves at the inlet of the channel is almost the same as fully developed annular flow in a straight pipe, which is the inlet initial condition for this channel. The followings are noted from these photos in Fig. 7. For the any flow rate of the gas and liquid phase, the interfacial waves seem smooth near the throat section as compared with near the inlet on the nozzle part or the outlet of the diffuser part. Especially, in the nozzle part where the cross sectional area of the channel gradually decreases, the special pattern of the interfacial waves gradually tend to disappear along the flow direction. This indicates that the wave height of interfacial waves become smaller in this part. In the nozzle part, the fluids were accelerated and the mean velocity of the gas-phase must finally reach up to four times of the inlet velocity due to the decreased cross sectional area. It is thought that the shear stress acting on the gas–liquid interface consequently becomes larger, so the interfacial waves were squeezed toward the pipe wall and modified to flatten.

4.2.2. Time-averaged velocity and fluctuation velocity profiles for transient annular flow

Fig. 8 show the measured gas-phase velocity profiles in the nozzle section, where the inner diameter of the channel is $\phi = 15$ mm, in which the flow is accelerating. The figure (a) shows the time-averaged velocity profiles and (b) represents the fluctuation velocity profiles, respectively. The horizontal axis represents the radial position from the central axis of the flow channel. The position of $r = 0$ mm indicates the central axis, $r = 7.5$ mm indicates the pipe wall of the throat section, respectively. In Fig. 8(a), the vertical axis means the time-averaged axial velocity non-dimensionalized by the superficial gas velocity defined in $\phi = 20.0$ mm I.D. pipe. In Fig. 8(b), vertical axis means the fluctuation velocity non-dimensionalized by the superficial gas velocity defined in $\phi = 15$ mm I.D. pipe, which corresponds to the diameter of the measuring part. Typical results of three cases are presented in Fig. 8. The open-symbols represent the results for the annular flow. The result for single-phase flow represented in solid-circled line was also plotted as a reference data.

From Fig. 8(a), the difference between the annular flow and the single-phase flow is not significant in time-averaged velocity profiles in the nozzle part. The velocity profiles in both cases were modified to flatten shape as compared with flows in a straight pipe as mentioned in Fig. 3(a). The power dependency on time-averaged velocity profiles in throat section becomes much smaller such as 1/14–1/18, which might be usually 1/7 in a straight pipe for fully developed single-phase flow. This is the nozzle rectification effect, which is well known phenomenon in single-phase

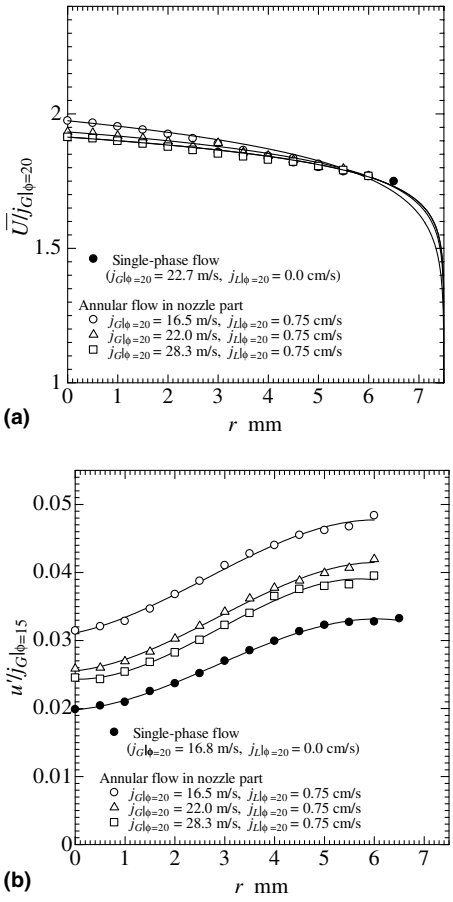

Fig. 8. Time averaged and fluctuation velocity profiles for the transient annular flow passing through the nozzle part of $\phi = 15$ mm. (a) Time-averaged velocity profiles. (b) Fluctuation velocity profiles.

flow passing through a reducer. In the case of the annular flow, the result shows that the rectification effect of nozzle part overcome the peaking effect, which modify the velocity profile more peaked observed in the fully developed annular flow in a straight pipe as mentioned in Fig. 3(a). From Fig. 8(b), it is noted that the fluctuation velocity for the single-phase flow in the nozzle section is much suppressed as compared with equilibrium state single-phase flow in a straight pipe shown in Fig. 3(b). The value of non-dimensionalized fluctuation is around 0.02, which is about a half of the equilibrium single-phase flow. Generally, the turbulence fluctuation velocity in the transient state passing through the nozzle part becomes smaller than that of the equilibrium state flow in a straight pipe due to the nozzle rectification effect. This phenomenon is well confirmed in the measured results for single-phase flow as shown in Fig. 8(b).

On the other hand, the fluctuation velocities for the annular flow in the nozzle part were much more enhanced, that is about one and half times compared with single-phase flow. This indicates that the liquid film flow with wavy interface must affect the enhancement of the turbulence fluctuation.

Fig. 9 show the velocity profiles measured in the throat part. Fig. 9(a) shows the time-averaged velocity profiles and (b) represents the fluctuation velocity profiles, respectively. From these figures, it is found that the velocity profile is modified much more flatten shape due to the nozzle rectification effect. This indicates the power-dependency of the time-averaged velocity profiles, which is approximately 1/30, becomes much smaller as compared with nozzle part. For the fluctuation velocity shown in Fig. 9(b), the value of fluctuation is about two times of single-phase flow. This indicates that the enhancement of turbulence fluctuation in annular flow due to the wavy interface is much more significant as compares with that of the nozzle section.

Fig. 10 show the velocity profiles measured in the diffuser part, which is located at the downstream of the throat part. In the diffuser part, the cross sectional area is increasing and the flow is decelerated. Fig. 10(a) shows the time-averaged velocity profiles. From Fig. 10(a) it is noted that the time-averaged velocity profiles in diffuser section has mountain-like shape. The velocity near the central axis is flattened shape, and gradually decreases near the wall region. This indicates the flatten velocity profiles in the throat part shown in Fig. 9(a) is left near the central axis, and velocity boundary layer is glowing near the wall

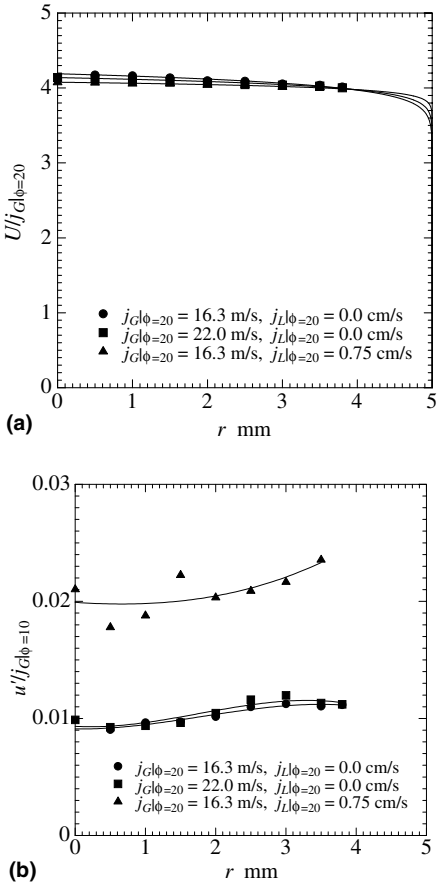

Fig. 9. Time averaged and fluctuation velocity profiles for the transient annular flow passing through the throat part of $\phi = 10$ mm. (a) Time-averaged velocity profiles. (b) Fluctuation velocity profiles.

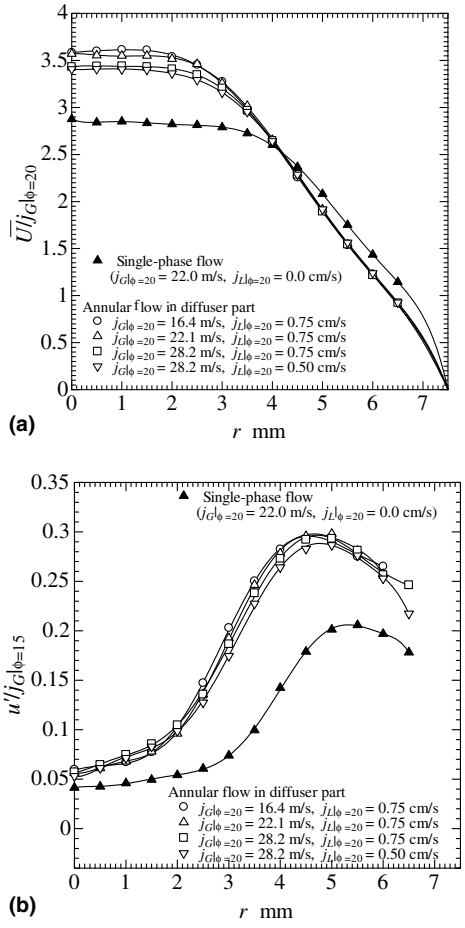

Fig. 10. Time averaged and fluctuation velocity profiles for the transient annular flow passing through the diffuser part of $\phi = 15$ mm. (a) Time-averaged velocity profiles. (b) Fluctuation velocity profiles.

region. In annular flow represented in open dots, the velocity near the central axis is increased and the velocity near the wall is decreases compared with single-phase flow. This is consistent with the results for fully developed annular flow as mentioned before in Fig. 3(a). Fig. 10(b) shows the turbulence fluctuation velocity profiles for the annular flow passing through a diffuser part. The turbulence fluctuation in the diffuser part is much more enhanced compared with fully developed flow in a straight pipe. This tendency is observed in both cases of the single-phase flow and the annular flow. This indicates the turbulence fluctuation energy is increased as the mean velocity is decelerated. These phenomena are unique in transient flow, where the flow is not reach an equilibrium state. The fluctuation velocity profiles has a peak around the radial position is about 4–5 mm. The fluctuation of $r = 4$–5 mm is much more increased. This region corresponds to the strong share layer formed between the gas-core flow from the throat part and the ambient stagnant region near the wall. The fluctuation velocity in annular flow is much more enhanced compared with single-phase flow. This means the wavy interface on liquid film affects the additional fluctuation on gas-phase in annular two-phase flow.

4.2.3. Liquid film thickness distribution around the throat section

Fig. 11 shows the liquid film thickness distribution along the flow direction passing through the nozzle, throat and diffuser part. The horizontal axis indicates the distance from the inlet of the nozzle part. The position of the 0–100 mm corresponds to the nozzle part, 100–120 mm corresponds to the throat part and 120–220 mm is the diffuser part, respectively. The measurement station in diffuser part is attached at the position of 170 mm from the inlet of the test channel, so the horizontal scale is represented from 0 mm to 170 mm. Fig. 11(a) is the typical results for the case of the gas-phase superficial velocity is relatively small, where the disturbance wave occurs. (b) is the result for the ripple region in which the gas-phase velocity is relatively high and liquid flow rate is relatively small. The symbols of circle indicate the base film thickness distribution, the triangles represent the mean film thickness and rectangle indicate the maximum film thickness, respectively.

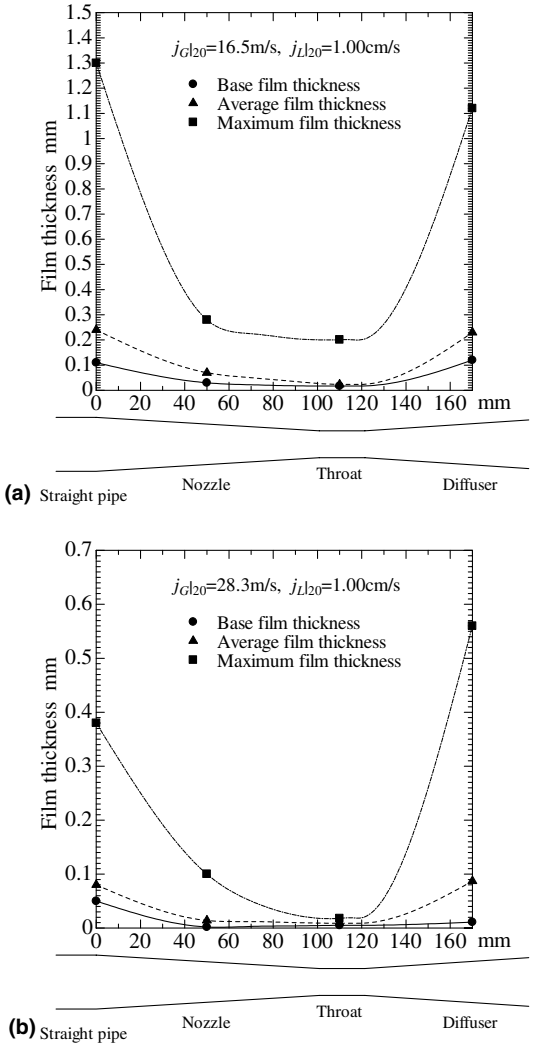

Fig. 11. Liquid film thickness distribution around the throat section (a): disturbance wave region, (b): ripple region. (a) Result for the disturbance wave region ($j_{G|20} = 16.5$ m/s, $j_{L|20} = 1.00$ cm/s). (b) Results for the ripple region ($j_{G|20} = 28.3$ m/s, $j_{L|20} = 1.00$ cm/s).

From Fig. 11, it is noted that the film thickness is extremely decreased along the nozzle part, and reaches the minimum at the throat, where the cross sectional area becomes minimum in the channel, and regain in the diffuser part. The mean film thickness in the throat part is about 1/10 of the fully developed flow in a straight pipe. As the film thickness is mainly depends on the gas-core velocity as mentioned above, the results obtained in nozzle-throat-diffuser part is qualitatively consistent with previous results obtained in fully developed flow. But in the diffuser part, which locates in the downstream of the throat, the film thickness is regained and much more increased as compared with the nozzle part even though the superficial velocity is the same each other. The reason of the difference of film thickness between the nozzle and diffuser part is due to the difference of the gas-core velocity profiles, especially, the velocity gradient near the wall region. This causes the difference of the shear stress acting on the liquid film interface.

In the case for the disturbance wave region shown in (a), the maximum wave height is relatively large even in the throat part. This is in clearly contrast compared with ripple region shown in (b). This indicates that the disturbance wave, which has very large wave height, survive even in the throat part where the strong share stress act to the liquid film interface. This result consistent with the result of the direct observations as mentioned in Fig. 7.

5. Conclusions

Experimental studies on turbulence modification in annular two-phase flow passing through a throat section were carried out. Followings are noted from the results. (1) In fully developed annular flow in a straight pipe, the time-averaged velocity profiles are modified to sharpened shape compared with the single-phase flow. (2) The fluctuation velocity becomes larger than that of the single-phase flow through the whole radial position. (3) The turbulence in annular flow is modified to the coherent structure in relatively low-frequency region, which should be affected by gas–liquid wavy interface, which is periodically moving on liquid film flow. (4) In the throat part, the liquid film thickness becomes significantly smaller. (5) In the nozzle and the throat part, the time-averaged velocity profiles are modified to flatten due to the nozzle rectification effect. This tendency is nearly the same in both cases in annular flow and single-phase flow. (6) In the nozzle and the throat part, the fluctuation velocity is much enlarged in annular flow due to the wavy interface on the liquid film flow. (7) In the diffuser part, the gas-core velocity distribution is modified to the mountain-like shape. The fluctuation velocity is much more enhanced in the strong share layer region formed between the high-speed gas-core flow and the peripheral stagnant flow. (8) The liquid film thickness in the diffuser part is much more increased compared with the nozzle part. This is due to the difference of the gas-core velocity distribution.

References

Azzopardi, B.J., Teixeira, J.C.F., 1994a. Trans. ASME J. Fluids Eng. 116, 796–800.
Azzopardi, B.J., Teixeira, J.C.F., 1994b. Trans. ASME J. Fluids Eng. 116, 792–795.
Azzopardi, B.J., 1999. Int. J. Multiphase Flow 25, 945–955.
Fore, L.B., Dukler, A.E., 1995. Int. J. Multiphase Flow 21 (2), 137–149.
Gore, R.A., Crowe, C.T., 1989. Int. J. Multiphase Flow 15 (2), 279–285.
Hestroni, G., 1989. Int. J. Multiphase Flow 15 (5), 735–746.
Ishii, M., Grolmes, M.A., 1975. AIChE J. 21, 308.
Kajishima, T., Takiguchi, S., Miyake, Y., 1999. Recent Advances in DNS and LES. Kluwer Academic, pp. 235–244.
Kutateladze, S.S., 1972. Fluid. Mech.—Soviet, Res. 1, 29.
Laufer, J., 1954. NACA Report, 1174.
Raynolds, A.J., 1974. Turbulent Flows in Engineering. John Wiley & Sons.
Serizawa, A., Kataoka, I., Michiyoshi, 1992. Multiphase Sci. Technol. 6, 257–301.
Steen, D.A., Wallis, G.B., 1964. AFC Report NYO-3114-2.